SI Appendix for

Structural Basis for mRNA Surveillance by Archaeal Pelota and GTP-bound EF1α Complex

Kan Kobayashi, Izumi Kikuno, Kazushige Kuroha, Kazuki Saito,
Koichi Ito, Ryuichiro Ishitani*, Toshifumi Inada, and Osamu Nureki*

*To whom reprint requests should be addressed. E-mail: nureki@ims.u-tokyo.ac.jp, ishitani@ims.u-tokyo.ac.jp

Discussion

The NSD mediated by the Dom34·Hbs1 complex

In no-go decay (NGD), the translational elongation of ribosome is blocked by stable mRNA structures or by a cluster of rare codons, and subsequently the mRNA is endonucleolytically cleaved near the stalled site (1). Recently, we have found that the synthesis of consecutive basic amino-acid polypeptide blocks translational elongation, inducing NGD (2). The Dom34·Hbs1 complex is not strictly required for this NGD process (2).

The endonucleolytic cleavage by NGD produces 3'-truncated mRNAs. In wild type cells, the resultant 5'-capped mRNA lacking stop codons (nonstop mRNA) is rapidly degraded by 3'-to-5' exonucleolytic pathway, while it is rather stable in the *ski2*Δ mutant in which the 3'-to-5' degradation pathway is impaired. We have found that the protein production from the nonstop mRNA is largely dependent on the Dom34·Hbs1 complex. To further confirm how the Dom34·Hbs1 complex is involved in the protein production from the nonstop mRNA, we constructed reporter gene system (Fig. S9A), in which a hammerhead ribozyme sequence (Rz) was inserted between *GFP* and *FLAG-HIS3* to form the in-frame *GFP-Rz-FLAG-HIS3* fusion gene. Transcription of *GFP-Rz-FLAG-HIS3* results in the production of 5'-capped nonstop *GFP-Rz* mRNA (Fig. S9A). The result showed that protein synthesis from the nonstop *GFP-Rz* mRNA is largely dependent on the Dom34·Hbs1 complex in the *ski2*Δ background (Fig. S9B, upper panel, lanes 6 and 8), although the amount of the truncated GFP mRNA only decreased moderately (2-fold) by the deletion of *DOM34* (Fig. S9B, lower panel, lanes 5-8). Thus the NSD activity by the Dom34·Hbs1 complex can be reasonably evaluated from the protein synthesis from the nonstop mRNA template in the *ski2*Δ background. Therefore, these results strongly suggest that the Dom34·Hbs1 complex is predominantly required for the translation of nonstop mRNA. Combined with the present structural analysis, it is probable that the efficient dissociation of the stalled ribosome from the 3' end of nonstop mRNA by the Dom34·Hbs1 complex facilitates recycling of the nonstop mRNA template and release of premature protein product (Fig. S9C).

Molecular mimicry of the ribosome-bound tRNA in the A/T state

Our recent study suggested that aEF1α is involved in three different processes: translational elongation and termination, and the mRNA surveillance pathway (3). Moreover, the present structure revealed that the mode of interaction between aPelota and aEF1α is similar to that between aa-tRNA and EF-Tu. Therefore, aEF1α may equally bind to and deliver the three different factors (*i.e.* aa-tRNA, aRF1, and aPelota) to the ribosomal A site. This idea prompted us to compare the present structures to the recently reported crystal structure of the aa-tRNA·EF-Tu complex bound to the ribosome (4), which captured the initial step of translational elongation.

In the ribosome, the structure of the EF-Tu bound tRNA is distorted, as compared to that in the isolated aa-tRNA·EF-Tu complex (4). In this "A/T" conformation, the tRNA anticodon stem is bent and the spatial arrangement of the D stem versus the acceptor-T stem is changed, resulting in a bend of approximately 30° in the tRNA body. This tRNA distortion in the A/T state is considered to be important for sampling the correct codon-anticodon pairing, which directly couples the codon recognition to the GTPase activation of EF-Tu.

Intriguingly, the present structure of aPelota bound to aEF1α is more similar to that of the A/T state tRNA than to the tRNA in the isolated aa-tRNA·EF-Tu complex (Fig. S10). Especially, the spatial arrangement of domain A versus domain C of aPelota resembles that of the anticodon arm versus the T arm of the A/T state tRNA. The NGD and NSD processes start with the entrance of the Pelota/Dom34·Hbs1 complex into the empty A site of a ribosome stalled by an aberrant mRNA, which may occur irrespective of the mRNA codon in the decoding center. Therefore, the overall structure of aPelota, and probably that of Pelota/Dom34 as well, in complex with aEF1α or Hbs1, already adopts the bent conformation mimicking the A/T state tRNA (Fig. S10B) prior to the interaction with the ribosome. This mimicry of the A/T state tRNA may facilitate the entrance into the A site of the stalled ribosome without structural changes.

Role of the GTPase activities of Hbs1 and aEF1α in the mRNA surveillance pathways

In the normal elongation cycle of the ribosome, correct codon recognition by the tRNA anticodon is sensed by the decoding center of the 16*S* rRNA, which triggers the GTPase activity of EF-Tu (4-6). These two events may be coupled by a global conformational change of the ribosome, as well as the structural flexibility of the tRNA.

In contrast to the tRNA, the interaction between domains A and C of Pelota seems

stable, and includes many salt bridges and hydrophobic interactions. In addition, the arrangements of domains A and C are almost the same in the three crystal structures of aPelota and Dom34, despite the differences in their amino acid sequences and crystal packing, supporting this structural rigidity. Therefore, this structural rigidity implies that the GTPase activation of Hbs1 (and aEF1α) by Pelota may not be rapidly coupled to the binding of the complex to the ribosomal A site. This hypothesis is consistent with our recent finding that the GTPase activation of aEF1α by aPelota is significantly weaker than that by aRF1 (3).

The question then arises as to the role of the GTPase activities of Hbs1 and aEF1α in the mRNA surveillance pathways. To address this question, we analyzed the NGD and NSD activities of yeast Hbs1 mutants deficient in the GTPase activity (T232A and H255A; corresponding to Thr71 and His94 of aEF1α, respectively) (Fig. S1). Interestingly, both of these mutants showed a complete loss of the NSD activity, and moderately impacted the NGD activity. These results thus suggest that the disruption of the Hbs1 GTPase activity does not affect the recruitment of the putative endonuclease for NGD. This is consistent with the previous result that the deletion of Hbs1 is not critical for the endonucleolytic cleavage of the NGD substrate (1). Our recent finding suggested that Pelota/Dom34 and Hbs1 are even dispensable for NGD generated by a run of Arg or Lys codons, which blocks elongation more robustly than a stem-loop structure (2). In contrast, the accumulation of nonstop mRNA products, which requires the disassembly and recycling of the stalled ribosome, was severely affected by the Hbs1 mutants deficient in GTPase activity. Therefore, this weak (and slow) GTPase activation of Hbs1 (and aEF1α) by Pelota may be essential for the latter process, the disassembly and recycling of the stalled ribosome. We speculate that this slow GTPase activity may act as a timekeeper to delay the progress of the NGD process, ensuring the hydrolysis of the aberrant mRNA by the recruitment of the putative endonuclease.

Destabilization mechanism of the stalled ribosome

The present functional analyses revealed that the GTPase activation of Hbs1 is important for the disassembly of the stalled ribosome. By analogy with the translational elongation cycle, it is likely that Pelota may undergo some structural changes along with the ribosome after the GTP hydrolysis by Hbs1. One possibility is that the Pelota-bound ribosome is driven toward a state similar to the A/A or A/P states as in the elongation cycle. However, Pelota domain C has a bulkier and more protruding structure as compared to the corresponding T loop of tRNA (Figs. 2A and S10) that intimately

interacts with the L11 region and helices H38 and H84 of the 23*S* rRNA in the A/T, A/A, and P sites, respectively (4, 7). Therefore, in this process, the protrusion of Pelota domain C would interact with the rRNA residues of the large ribosomal subunit around the A and P sites, including the L11 region, and helices H38 and H84 (Fig. S11A), thereby inducing the destabilization of the ribosomal subunits.

Insights into the NGD and NSD pathways

Based on the present crystal structure and functional analyses, we propose the following mechanism of the NGD and NSD mRNA surveillance pathways (Fig. S11B). Firstly, the translational elongation cycle is arrested by the NGD and NSD substrates, which will result in stalled ribosomes within the mRNA (Fig. S11B-I) and at the 3'-end of the mRNA (Fig. S11B-II), respectively. In both cases, the Pelota·Hbs1 complex binds to the empty A site of the stalled ribosome (Fig. S11B-III). The mutations that affect the Pelota·Hbs1 complex formation (Y300A) or the recognition of the stalled ribosome [K2A, F47A, and Δ(F47-T60)] reduced both the NGD and NSD activities (Fig. 4), suggesting the inhibition of all of the downstream processes. Secondly, the binding of the complex locks the stalled ribosome (Fig. S11B-III), which may suppress mistranslation by preventing the entrance of a non-cognate tRNA into the A site. The GTP hydrolysis by Hbs1 is quite slow, so there is sufficient time for the recruited endonuclease to access and cleave the NGD substrate (Fig. S11B-IV). The NGD cleavage product was still detected with the mutations of Hbs1 (T232A and H255A) and Pelota Loop B [(D90-P100)A] (Fig. 4), suggesting the minor effect of these mutants on the recruitment of the endonuclease. However, in these mutants, the final processes, including the ribosomal disassembly, were inhibited, which may have resulted in the reduction of the NSD activity. Finally, the GTP hydrolysis by Hbs1 and the putative structural change of Pelota may destabilize the ribosomal subunits (Fig. S11B-V), which would ultimately induce the disassembly of the stalled ribosome.

Materials and Methods

Sample preparation

The genes encoding full-length *Aeropyrum pernix* aEF1α and aPelota were cloned into pET15b vectors (Novagen) and expressed in the *Escherichia coli* BL21(DE3)CodonPlus strain as N-terminal His-tagged proteins. Cells were grown at

37ºC to an A_{600} of 0.5–0.7, and then protein expression was induced with 0.5 mM isopropyl-β-D-thiogalactopyranoside at 20ºC overnight. aPelota was purified as described below. Cells were harvested and suspended in buffer A (20 mM Tris-HCl, pH 8.0, 200 mM NaCl, 10 mM imidazole, 1 mM 2-mercaptoethanol, 0.1 mM phenylmethylsulfonyl fluoride), and lysed by sonication. After centrifugation, the supernatant was incubated at 70ºC for 30 min, and then centrifuged again. The supernatant was separated from the protein pellets, and applied to a column of Ni-NTA Superflow (Qiagen). The column was washed with buffer A containing 20 mM imidazole, and aPelota was eluted with buffer A containing 250 mM imidazole. The eluted fraction was dialyzed against buffer B (50 mM Tris-HCl pH 8.0 and 100 mM NaCl), and then applied to an ion-exchange Resource S column (GE Healthcare) equilibrated with buffer C (50 mM Tris-HCl, pH 8.0, 50 mM NaCl and 1 mM DTT). aPelota was eluted by a linear gradient of NaCl from 50 to 600 mM. Fractions containing aPelota were collected and dialyzed against buffer D (25 mM Tris-HCl, pH 8.0, 500 mM NaCl and 1 mM DTT). Purification of aEF1α was performed by essentially the same procedure as described above, except that the His-tag was cleaved with thrombin before the Resource S column chromatography, and the protein was further purified by Hiload 16/60 Superdex 200 gel filtration chromatography (GE Healthcare) after the Resource S step. The Hiload 16/60 Superdex 200 resin was equilibrated with buffer E (25 mM Tris-HCl, pH 8.0, 500 mM NaCl and 1 mM 2-mercaptoethanol). SeMet-labeled aEF1α was expressed in the B834(DE3)CodonPlus strain and was purified by the same procedure as for the native protein.

Crystallization and data collection

aPelota and aEF1α were concentrated by ultrafiltration to 39 mg/ml and 28 mg/ml respectively, and then were mixed at a molar ratio of 1:1. Crystals of the aPelota·aEF1α·GTP complex were grown by the sitting drop vapor diffusion method at 20ºC by mixing equal amounts of the protein solution (17 mg/ml aEF1α and 15 mg/ml aPelota, and 5 mM GTP) and the reservoir solution (2.2 M NaCl, 100 mM imidazole, pH 8.0). The complex of SeMet-labeled aEF1α, native aPelota and GTP was crystallized under the same conditions as for the native complex. The crystals were cryoprotected in 20% ethyleneglycol, 2.6 M NaCl, and 120 mM imidazole, pH 8.0, and were flash-cooled at 100 K. Diffraction data were collected at beamline NW12A at KEK PF-AR (Tsukuba, Japan), and were processed with the program HKL2000 (HKL Research). The statistics of the data collection are summarized in Supplementary Table SI.

Structure determination and refinement

Despite the sequence similarity between *A. pernix* aEF1α and *Sulfolobus solfataricus* aEF1α (8), as well as that between *A. pernix* aPelota and *Thermoplasma acidophilum* aPelota (9), our attempts to solve the structure by molecular replacement were unsuccessful. Therefore, the structure was determined by the single wavelength anomalous diffraction method, using the selenium anomalous signal. Fifty selenium sites were identified in one asymmetric unit by the program SnB (10). Heavy-atom refinement and phase calculations were performed with the program SHARP (11) using the reflections up to 3.2 Å, followed by solvent flattening with the program SOLOMON (12). The resulting electron density map allowed us to identify four complexes of aPelota·aEF1α in one asymmetric unit. Initial phases were extended up to 2.8 Å and improved by 4-fold NCS averaging with the program DM (13), which allowed automated model building with the program RESOLVE (14). The model was subsequently improved through alternating cycles of manual building using the program COOT (15) and refinement with the program PHENIX (16), after 5% of the reflections were set aside to calculate the R_{free}. The final model was refined against the native dataset up to 2.3 Å resolution to an R_{work} of 20.7%, with an R_{free} of 26.5%. The statistics of the phase calculation and structure refinement are summarized in Supplementary Tables SI and SII. The structure factors and coordinates of the aPelota·GTP·aEF1α complex have been deposited in the Protein Data Bank (accession code 3AGJ).

Measurement of the activities of Dom34 and Hbs1 mutants in nonstop mRNA translation and NGD

To measure the activities of Dom34 and Hbs1 mutants in nonstop mRNA translation, W303*ski2*Δ*dom34*Δ or W303*ski2*Δ*hbs1*Δ cells harboring a plasmid expressing the indicated Dom34 or Hbs1 mutants and the p416*GPDp-GFP-Rz-FLAG-HIS3* plasmid (2) were grown on SC medium. Two oligonucleotides (5'-CTAGCCCTGTCACCGGATGTGTTTTCCGGTCTGATGAGTCCGTGAGGACG AAACAGGA-3' and 5'-CTAGTCCTGTTTCGTCCTCACGGACTCATCAGACCGGAAAACACATCCGGT GACAGGG-3') were annealed and inserted into the SpeI site of pSA144 (p*GPDp-GFP-FLAG-HIS3-CYC1ter*) (17) to construct the p416*GPDp-GFP-Rz-FLAG-HIS3*. The relative levels of those products were determined by western blotting, using samples from W303 cell harboring

p416*GPDp-GFP-FLAG-HIS3* as a standard curve. To measure the activities of the Dom34 and Hbs1 mutants in NGD, W303*ski2*Δ*dom34*Δ or W303*ski2*Δ*hbs1*Δ cells harboring a plasmid expressing the indicated Dom34 or Hbs1 mutant and the p416*GPDp-GFP-SL-FLAG-HIS3* plasmid (18) were grown on SC-Ura medium, and RNA samples were prepared. The relative levels of *GFP-SL-FLAG-HIS3* and truncated 5'-*GFP* mRNAs were determined by a northern blot analysis using the samples from W303*ski2*Δ cell harboring p416*GPDp-GFP-SL-FLAG-HIS3* as a standard curve. The cleavage efficiency was estimated by the ratio between the total mRNA (full length mRNA and the truncated 5' *GFP* fragment) and the truncated 5' *GFP* fragment.

Figures

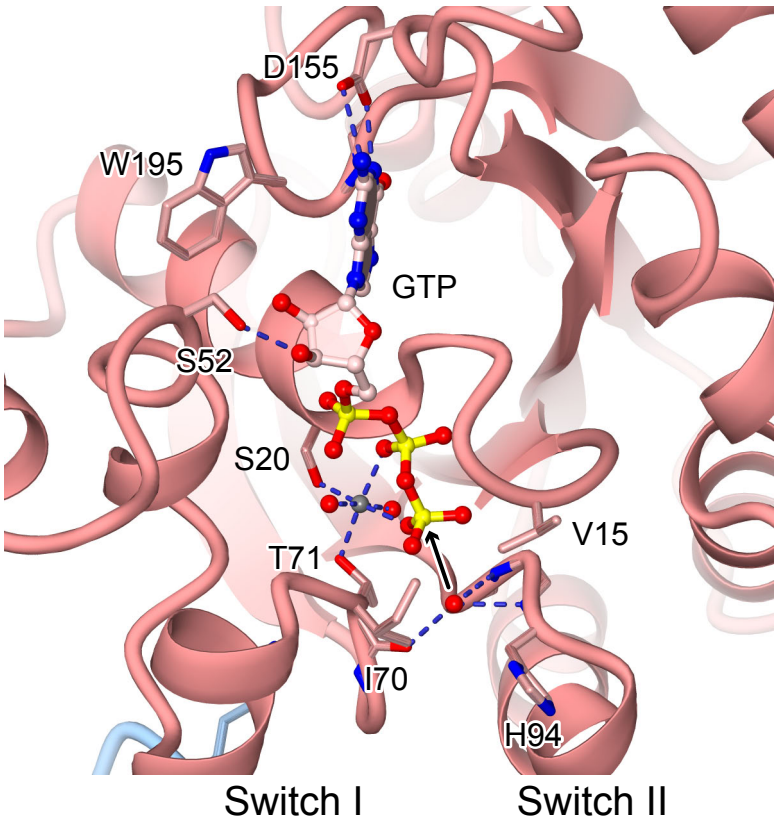

Fig. S1

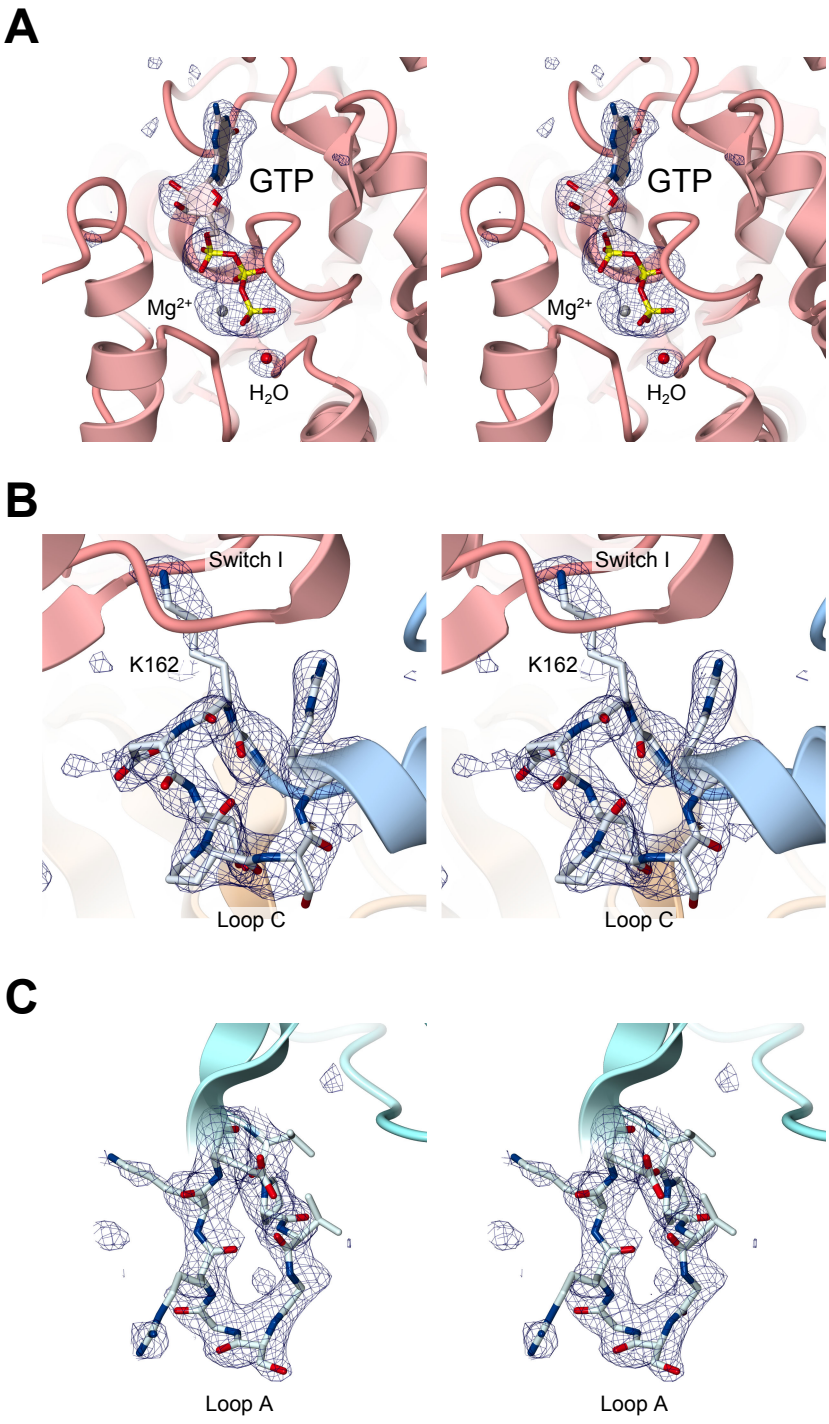
A
GTP
Mg^{2+}
H_2O
GTP
Mg^{2+}
H_2O
B
Switch I
K162
Loop C
Switch I
K162
Loop C
C
Loop A
Loop A

Fig. S2

A Site 1

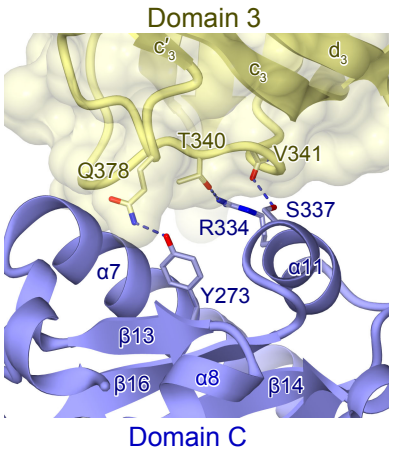

B Site 2

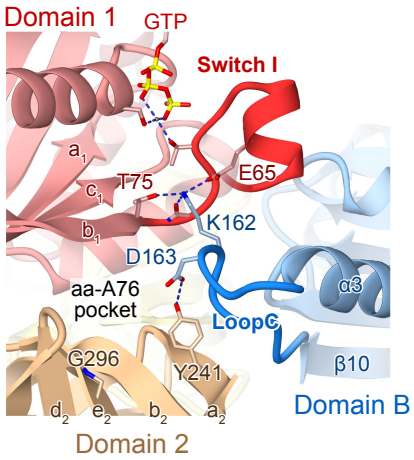

C Site 2

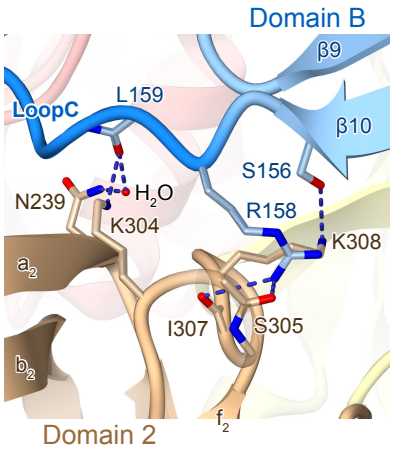

D Site 3

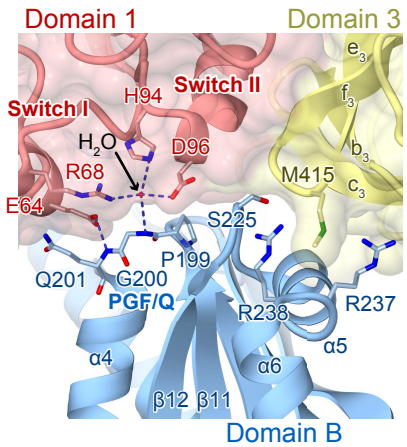

E Site 3

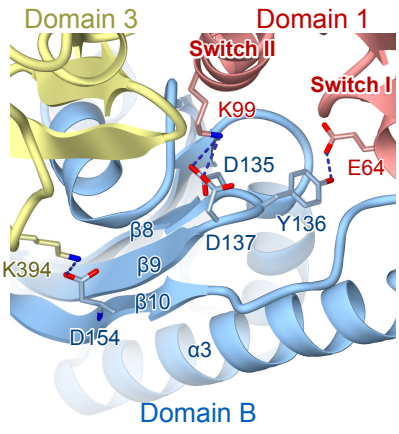

Fig. S3

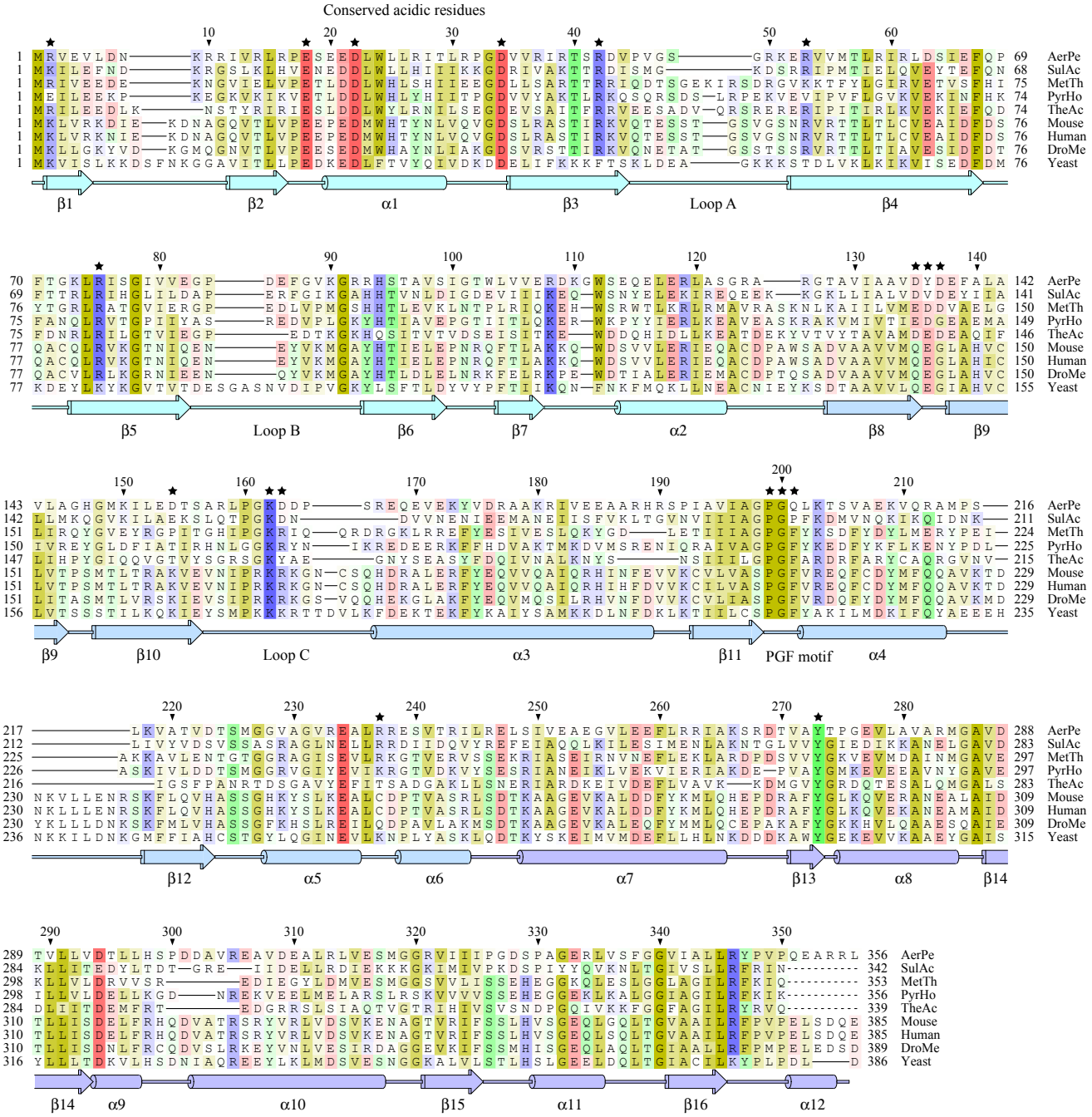
Conserved acidic residues
AerPe
SulAc
MetTh
PyrHo
TheAc
Mouse
Human
DroMe
Yeast
β1
β2
α1
β3
Loop A
β4
β5
Loop B
β6
β7
α2
β8
β9
β10
Loop C
α3
β11
PGF motif
α4
β12
α5
α6
α7
β13
α8
β14
α9
α10
β15
α11
β16
α12

Fig. S4

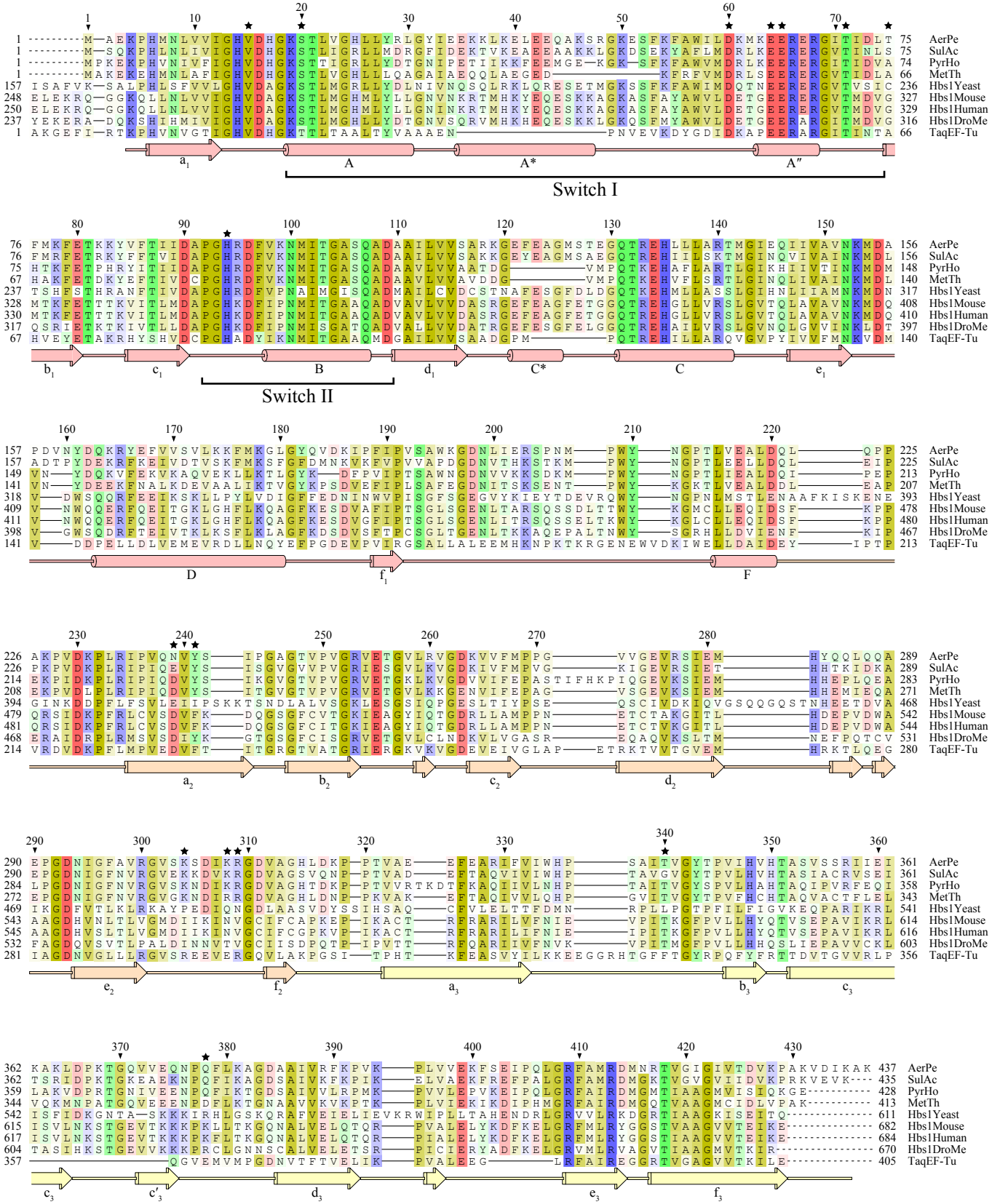
Switch I
Switch II
AerPe
SulAc
PyrHo
MetTh
Hbs1Yeast
Hbs1Mouse
Hbs1Human
Hbs1DroMe
TaqEF-Tu

Fig. S5

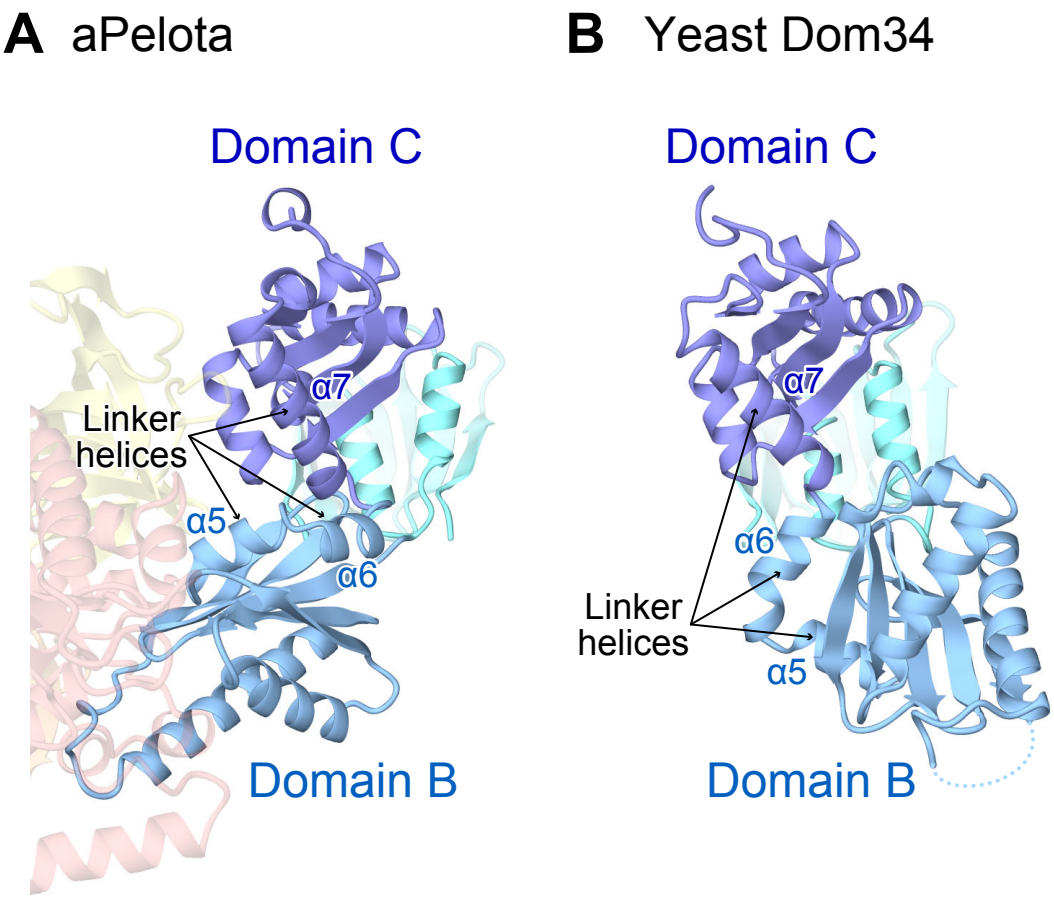
A aPelota
B Yeast Dom34
Domain C
Domain C
α7
α7
Linker
helices
α5
α6
α6
Linker
helices
α5
Domain B
Domain B

Fig. S6

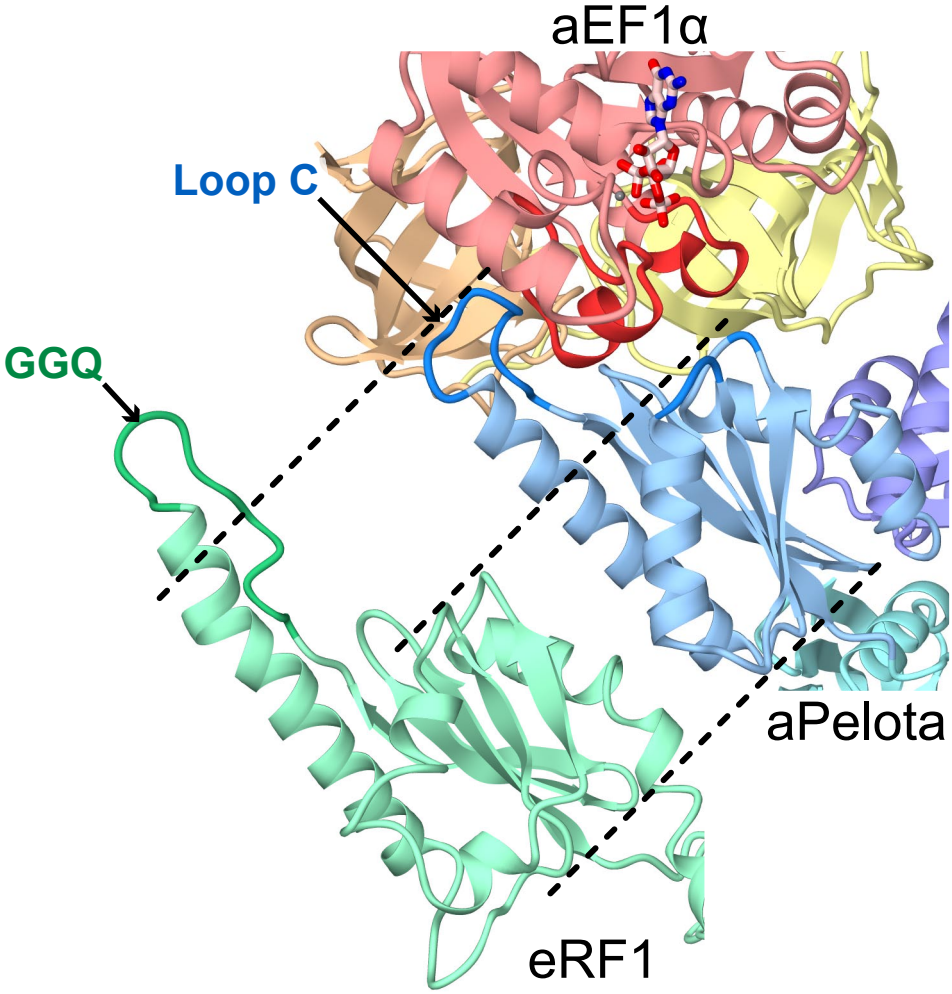

Fig. S7

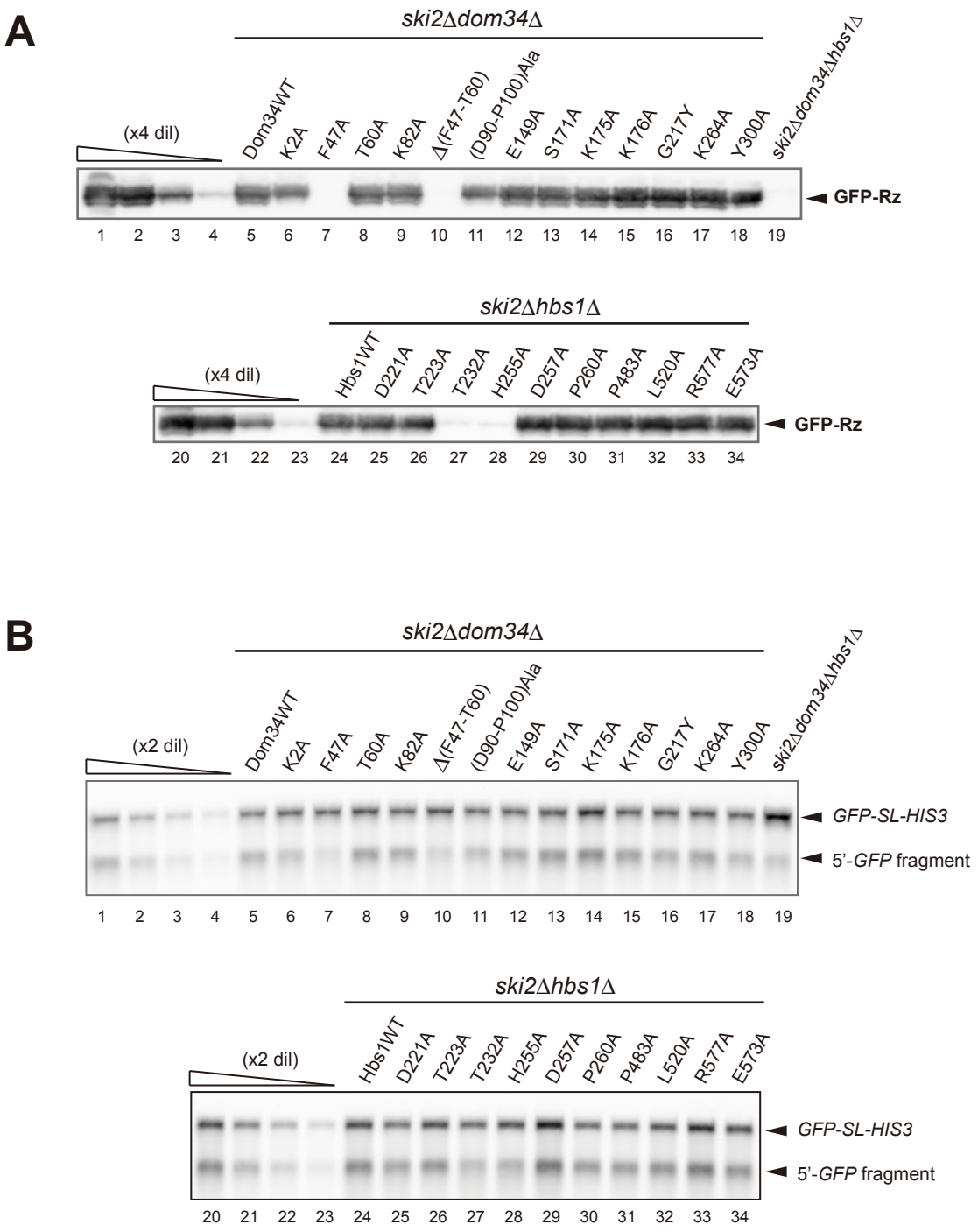
A
ski2Δdom34Δ
(x4 dil)
Dom34WT
K2A
F47A
T60A
K82A
Δ(F47-T60)
(D90-P100)Ala
E149A
S171A
K175A
K176A
G217Y
K264A
Y300A
ski2Δdom34Δhbs1Δ
GFP-Rz
1 2 3 4 5 6 7 8 9 10 11 12 13 14 15 16 17 18 19
ski2Δhbs1Δ
(x4 dil)
Hbs1WT
D221A
T223A
T232A
H255A
D257A
P260A
P483A
L520A
R577A
E573A
GFP-Rz
20 21 22 23 24 25 26 27 28 29 30 31 32 33 34
B
ski2Δdom34Δ
(x2 dil)
Dom34WT
K2A
F47A
T60A
K82A
Δ(F47-T60)
(D90-P100)Ala
E149A
S171A
K175A
K176A
G217Y
K264A
Y300A
ski2Δdom34Δhbs1Δ
GFP-SL-HIS3
5'-GFP fragment
1 2 3 4 5 6 7 8 9 10 11 12 13 14 15 16 17 18 19
ski2Δhbs1Δ
(x2 dil)
Hbs1WT
D221A
T223A
T232A
H255A
D257A
P260A
P483A
L520A
R577A
E573A
GFP-SL-HIS3
5'-GFP fragment
20 21 22 23 24 25 26 27 28 29 30 31 32 33 34

Fig. S8

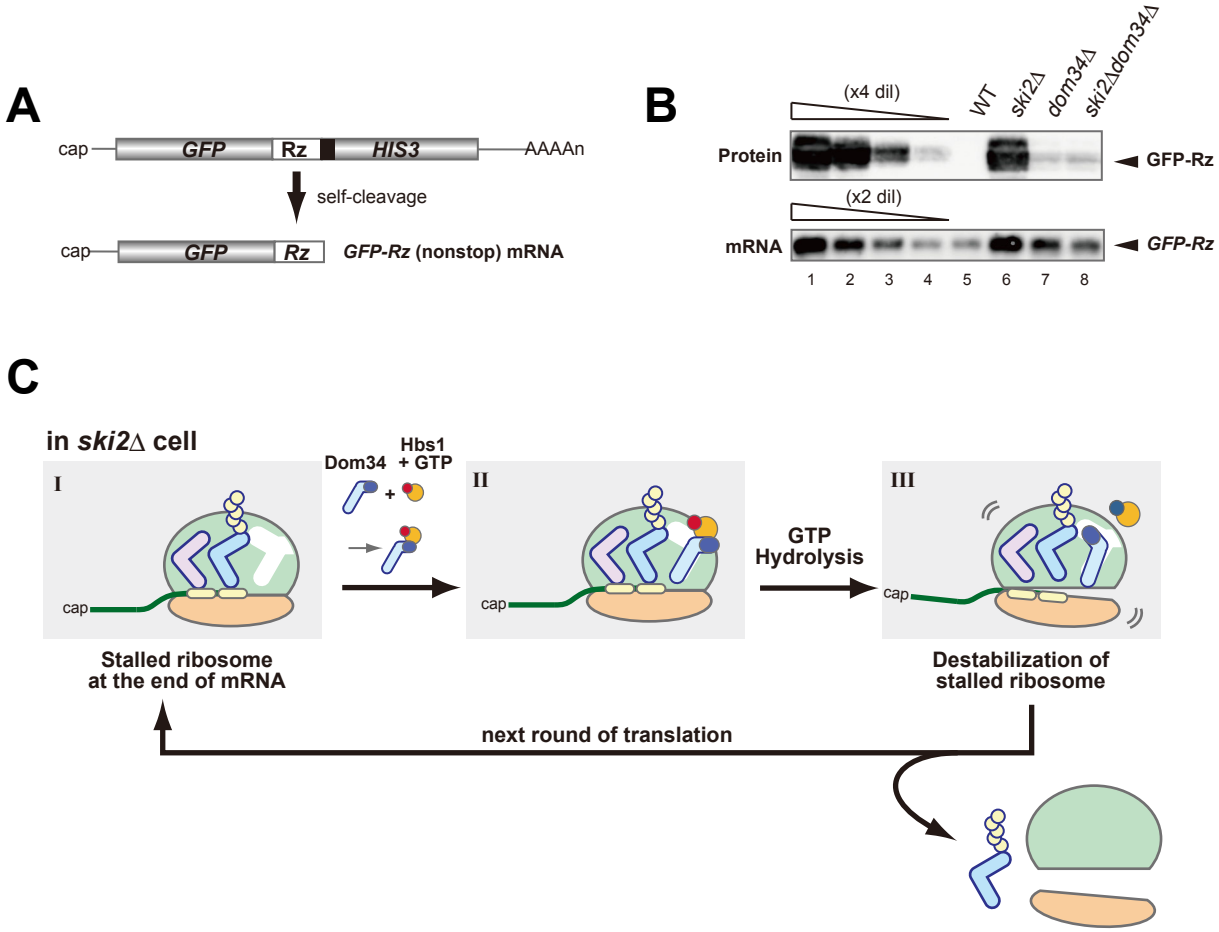
A
cap
GFP
Rz
HIS3
AAAAn
self-cleavage
cap
GFP
Rz
GFP-Rz (nonstop) mRNA
B
(x4 dil)
WT
ski2Δ
dom34Δ
ski2Δdom34Δ
Protein
GFP-Rz
(x2 dil)
mRNA
GFP-Rz
1 2 3 4 5 6 7 8
C
in ski2Δ cell
I
cap
Stalled ribosome
at the end of mRNA
Dom34
Hbs1
+ GTP
II
cap
GTP
Hydrolysis
III
cap
Destabilization of
stalled ribosome
next round of translation

Fig. S9

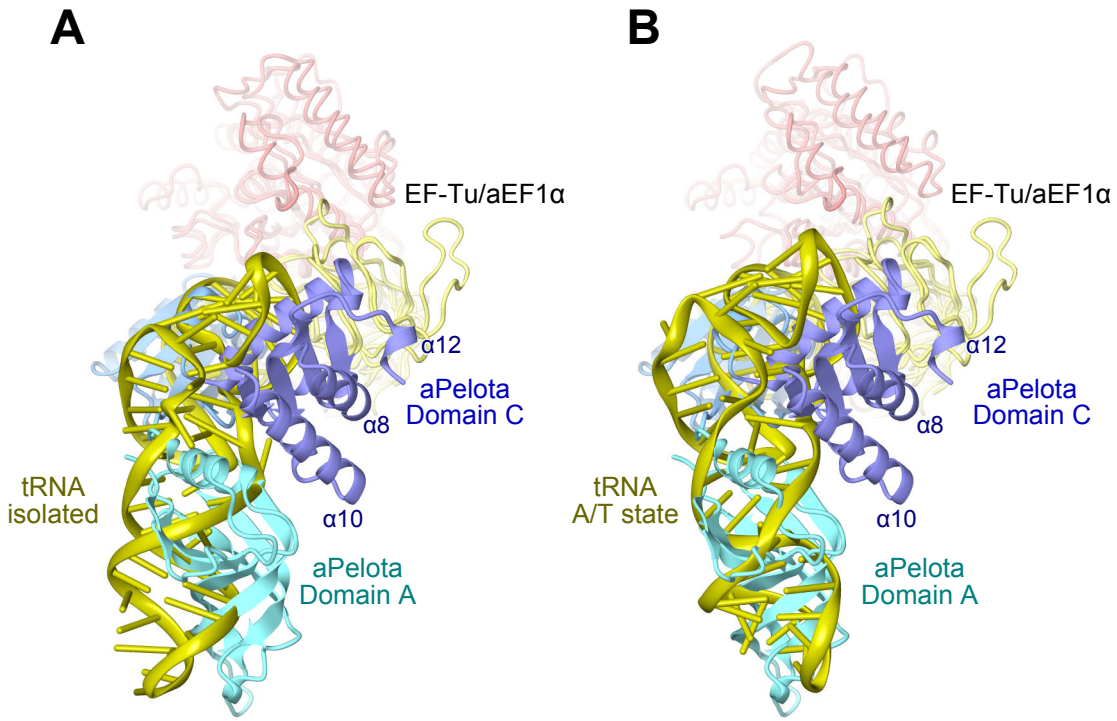
A
EF-Tu/aEF1α
α12
aPelota
Domain C
α8
tRNA
isolated
α10
aPelota
Domain A
B
EF-Tu/aEF1α
α12
aPelota
Domain C
α8
tRNA
A/T state
α10
aPelota
Domain A

Fig. S10

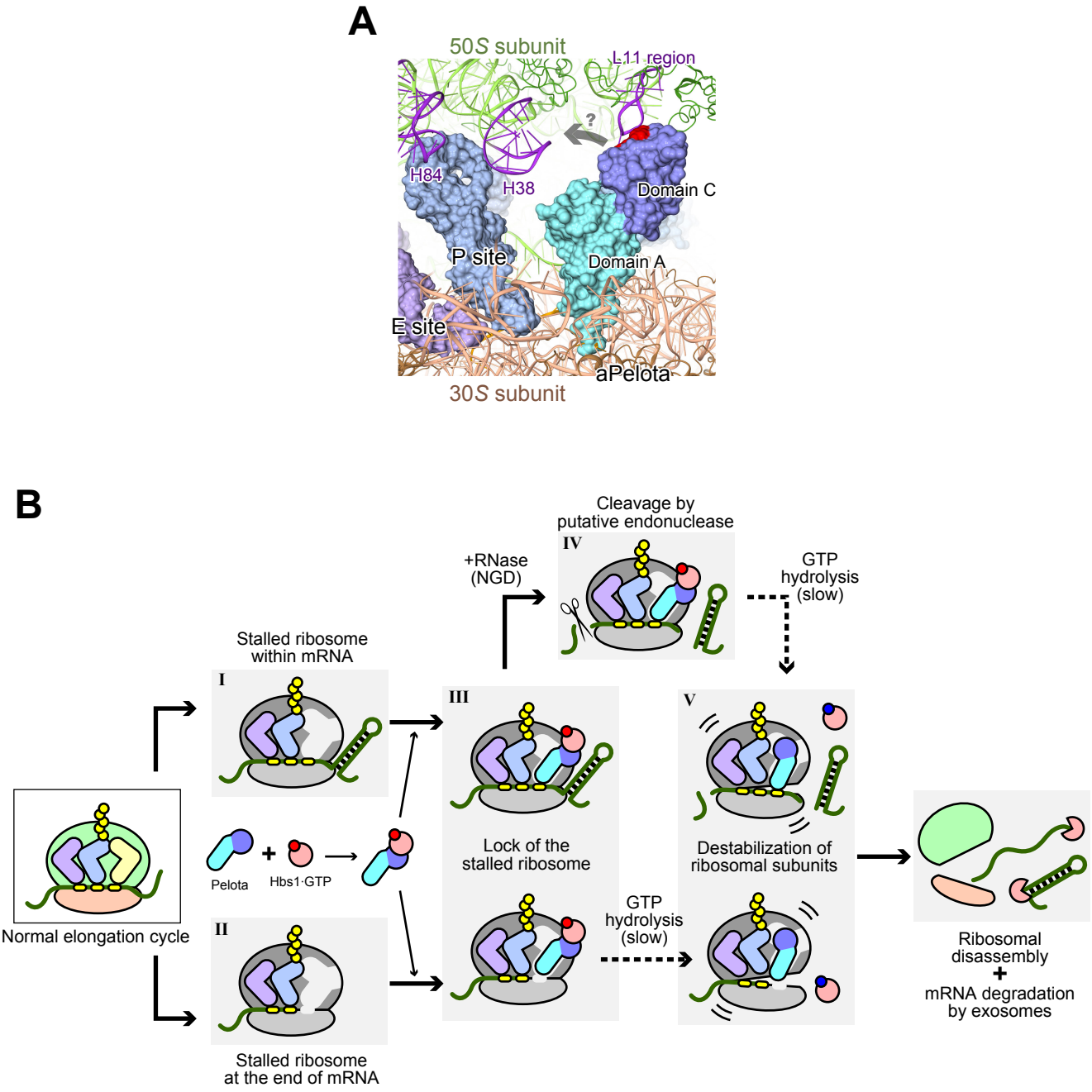
A
50S subunit
L11 region
?
H84
H38
Domain C
P site
Domain A
E site
aPelota
30S subunit
B
Cleavage by
putative endonuclease
IV
+RNase
(NGD)
GTP
hydrolysis
(slow)
Stalled ribosome
within mRNA
I
III
V
Lock of the
stalled ribosome
Destabilization of
ribosomal subunits
Pelota
Hbs1·GTP
Normal elongation cycle
II
GTP
hydrolysis
(slow)
Ribosomal
disassembly
+
mRNA degradation
by exosomes
Stalled ribosome
at the end of mRNA

Fig. S11

Figure Legends

Fig. S1

GTPase center of aEF1α complexed with aPelota. The bound GTP, water molecules, and magnesium ion are depicted by ball-and-stick models. The aEF1α residues involved in the GTP recognition are shown with stick models. Hydrogen bonds, salt bridges, and ion coordination are indicated by dashed blue lines. The possible nucleophilic attack of the γ-phosphate of GTP by the putative catalytic water molecule is shown by an arrow.

Fig. S2

Electron density maps of the aPelota·aEF1α·GTP ternary complex structure.

(A) Unbiased $m|\mathbf{F}_o|–D|\mathbf{F}_c|$ electron density map around the bound GTP molecule, contoured at 3 σ. For the calculation of the map, GTP, Mg^{2+}, and the putative catalytic water molecule were omitted from the model.

(B) Unbiased $m|\mathbf{F}_o|–D|\mathbf{F}_c|$ electron density map of Loop C of aPelota, contoured at 2.5 σ. For the calculation of the map, residues 162–167 of aPelota were omitted from the model.

(C) Unbiased $m|\mathbf{F}_o|–D|\mathbf{F}_c|$ electron density map of Loop A of aPelota, contoured at 2.5 σ. For the calculation of the map, residues 44–52 of aPelota were omitted from the model.

Fig. S3

Close-up views of the interaction sites between aPelota and aEF1α. Proteins are shown by ribbon models with the domains color-coded as in Fig. 2. Hydrogen bonds and salt bridges are indicated by dashed blue lines.

(A) The interactions between aPelota domain C and aEF1a domain 3 (Site 1). The solvent accessible surface of aEF1a domain 3, calculated by the program MSMS (19), is shown with semitransparent coloring.

(B) and (C) The interactions between aPelota domain B and aEF1α domains 1 and 2 (Site 2). The switch I region and Loop C are highlighted in red and blue, respectively.

(D) and (E) The interactions between aPelota domain B and aEF1α domain 1 and 3 (Site 3). In panel (D), the solvent accessible surface of aEF1α is shown with

semitransparent coloring.

Fig. S4

Amino-acid sequence alignment of eukaryotic and archaeal Dom34/Pelota proteins (AerPe for *Aeropyrum pernix*, SulAc for *Sulfolobus acidocaldarius*, MetTh for *Methanothermobacter thermautotrophicus*, PyrHo for *Pyrococcus horikoshii*, TheAc for *Thermoplasma acidophilum*, and DroMe for *Drosophila melanogaster*). Conserved amino acids are highlighted in blue for basic, red for acidic, green for hydrophilic, and dark yellow for hydrophobic residues. The residues discussed in the text are indicated with stars. The secondary structural elements of *A. pernix* aPelota are shown below the sequences, with their names. The structure-based sequence alignment was calculated using the program PROMALS3D (20).

Fig. S5

Amino-acid sequence alignment of Hbs1, aEF1α, and EF-Tu (AerPe for *Aeropyrum pernix*, SulAc for *Sulfolobus acidocaldarius*, MetTh for *Methanothermobacter thermautotrophicus*, PyrHo for *Pyrococcus horikoshii*, DroMe for *Drosophila melanogaster*, and TaqEF-Tu for *Thermus aquaticus* EF-Tu). Conserved amino acids are highlighted in blue for basic, red for acidic, green for hydrophilic, and dark yellow for hydrophobic residues. The residues discussed in the text are indicated with stars. The secondary structural elements of *A. pernix* aPelota are shown below the sequences, with their names. The structure-based sequence alignment was calculated using the program PROMALS3D (20).

Fig. S6

Comparison of the domain arrangements of domains B and C in (A) aPelota and (B) yeast Dom34. Proteins are shown by ribbon models, with the domains color-coded as in Fig. 1. The structures of aPelota and yeast Dom34 were aligned based on the structural similarity between domain C, using the SSM algorithm. In panel (A), aEF1α bound to aPelota is shown with semitransparent coloring.

Fig. S7

Comparison of domain B of aPelota and human eRF1. Proteins are depicted by ribbon models, with the domains color-coded as Fig. 1. eRF1 is also shown by a green ribbon model, and the GGQ motif is indicated by an arrow. The structures of aPelota domain B and eRF1 domain B were aligned based on their structural similarity, using the SSM algorithm. The corresponding positions in the structures are indicated by dashed lines.

Fig. S8

In vivo functional analyses of yeast Dom34 and Hbs1 mutants.

(A) The activities of Dom34 and Hbs1 mutants in nonstop mRNA translation. The relative levels of those products were determined by western blotting with anti-GFP antibodies. The samples from W303*ski2*Δ cell harboring p416*GPDp-GFP-Rz-FLAG-HIS3* were used as a standard curve. For quantification, the samples were diluted 5-fold and analyzed by western blotting.

(B) The activities of Dom34 and Hbs1 mutants in NGD. The relative levels of *GFP-SL-FLAG-HIS3* and truncated 5'-GFP mRNAs were determined by northern blot analysis with DIG-labeled GFP probe. The samples from W303*ski2*Δ cell harboring p416*GPDp-GFP-SL-FLAG-HIS3* as a standard curve.

Fig. S9

(A) Schematic drawing of the *GFP-Rz-FLAG-HIS3* reporter mRNA. The filled boxes and lines indicate the open reading frames and untranslated regions, respectively. The tracts of A indicate the poly(A) tail. The black box indicates FLAG epitope tag.

(B) W303, W303*ski2*Δ or W303*dom34*Δ, W303*ski2*Δ*dom34*Δ cells harboring indicated p416*GPDp-GFP-Rz-FLAG-HIS3* plasmids were grown on SC-Ura medium. The samples from W303*ski2*Δ cell harboring p416*GPDp-GFP-Rz-FLAG-HIS3* were used as a standard curve (lanes 1–4). Top: The levels of GFP-Rz products were determined by Western blotting with anti-GFP antibodies. Bottom: The levels of *GFP-Rz* mRNA were determined by Northern blotting with DIG-labeled *GFP* probe.

(C) Schematic representation of the proposed function of the Dom34·Hbs1 complex in translation of nonstop mRNA in the *ski2*Δ mutant.

Fig. S10

Comparison to EF-Tu-bound tRNA in (A) the isolated (21) (PDB ID: 1B23) and (B) the ribosome-bound A/T state (4) (PDB ID: 2WRQ) forms. tRNA are shown in yellow ribbon representations. Proteins are shown in ribbon (aPelota) and tube (EF-Tu and aEF1a) representations, color-coded by domains as in Fig. 1. Domains 2 and 3 of aEF1α in the present complex structure were superimposed on those of tRNA-bound EF-Tu in the isolated and ribosome-bound forms, respectively, using the SSM algorithm.

Fig. S11

(A) Possible interactions between rRNA and aPelota domain C. The bulky protrusion of aPelota domain C is highlighted in red. The helices of 23S rRNA discussed in the main text are colored purple.

(B) Schematic representation of the proposed NGD and NSD pathways based on the present study.

Tables

Table SI.

Data collection and phasing statistics.

Data collection statistics	**SeMet**	**Native**
X-ray source	PF-AR NW12A	PF-AR NW12A
Wavelength (Å)	0.97913 (peak)	1.0
Space group	$C222_1$	$C222_1$
Unit cell dimensions (Å, °)	a = 149.0, b = 158.6, c = 426.0 $\alpha = \beta = \gamma = 90$	a =148.9 , b = 158.9, c = 427.2 $\alpha = \beta = \gamma = 90$
Resolution (Å)	50–2.80 (2.85–2.80)	50–2.30 (2.33–2.30)
Unique reflections	122,732 (5,835)	216,696 (10,151)
Redundancy	7.5 (3.2)	4.8 (2.7)
Completeness (%)	98.6 (95.1)	95.8 (90.5)
$I/\sigma(I)$	16.6 (2.1)	18.2 (2.2)
R_{sym}	0.111 (0.444)	0.079 (0.361)
Phasing statistics		
No. of Se sites	50	
Phasing power (Ano)*	0.878	
R_{cullis} (Ano)*	0.856	
Mean FOM*	0.26	

The numbers in parentheses are for the last shell.

*For acentric reflections

Table SII.

Structure refinement statistics.

Refinement statistics	
Resolution (Å)	32.433–2.30
No. of reflections (all/test)	216,119/10,902
R_{work}/R_{free}	0.2070/0.2649
No. of atoms	
Protein	24,212
Ligand	132
Water	1,349
RMSD of	
Bond length (Å)	0.009
Bond angle (°)	1.288
Average *B* factor (Å)	
Protein	49.1
Ligand	50.0
Water	46.3
Ramachandran plot	
Most favored region (%)	87.4
Additionally allowed region (%)	11.8
Generously allowed region (%)	0.4
Disallowed region (%)	0.4

The numbers in parentheses are for the last shell.

Table SIII.

A comprehensive list of these interactions in Sites 1, 2, and 3.

aPelota residue	aPelota atom	aEF1α residue	aEF1α atom	distance (Å)
Site 1				
Tyr273	OH	Gln378	NE2	2.7
Arg334	NH1	Thr340	OG1	3.0
Ser337	OG	Val341	O	2.8
Site 2				
Lys162	NZ	Glu65	OE2	2.7
Lys162	NZ	Glu65	OE1	3.3
Lys162	NZ	Thr75	OG1	2.7
Lys162	NZ	Asp73	O	2.5
Lys162	CE	Thr75	OG1	3.1
Asp163	OD2	Tyr241	OH	3.1
Arg158	O	Lys304	NZ	3.1
Ser156	OG	Lys308	NZ	3.7
Arg158	NH1	Ser305	O	3.1
Arg158	NH1	Ile307	O	3.7
Site 3				
Gln201	N	Glu64	OE2	2.9
Gly200	CA	Arg68	NH1	3.1
Ser225	CB	Asn416	CG	3.3
Asp135	OD1	Lys99	NZ	3.7
Asp137	OD2	Lys99	NZ	3.5
Asp137	OD1	Arg309	NH1	3.2
Tyr136	OH	Glu64	OE1	2.9
Asp154	OD1	Lys394	NZ	2.8
Asp154	OD1	Lys394	CE	3.2
Asp154	OD2	Lys394	NZ	3.2
Arg238	NH2	Met415	CE	3.3

References

1. Doma, M. K. & Parker, R. (2006) Endonucleolytic cleavage of eukaryotic mRNAs with stalls in translation elongation. *Nature* 440**:**561-564.
2. Kuroha, K., Dimitrova, L., Tatematsu, T., Kanao S., Akamatsu, M., Ito, T., Kato, Y., Shirahige, K. & Inada, T. (2010) RACK1 stimulates nascent polypeptide-dependent translation arrest. *J. Biol. Chem.* (in press)
3. Saito, K., Kobayashi, K., Wada, M., Kikuno, I., Takusagawa, A., Mochizuki, M., Uchiumi, T., Ishitani, R., Nureki, O. & Ito, K. (2010) An omnipotent role of archaeal EF1α in translation elongation, termination and quality control of protein synthesis. *Proc. Natl. Acad. Sci. U. S. A.* (in press)
4. Schmeing, T. M., Voorhees, R. M., Kelley, A. C., Gao, Y. G., Murphy, F. V., Weir, J. R. & Ramakrishnan, V. (2009) The Crystal Structure of the Ribosome Bound to EF-Tu and Aminoacyl-tRNA. *Science* 326**:**688-694.
5. Ogle, J. M., Brodersen, D. E., Clemons, W. M., Tarry, M. J., Carter, A. P. & Ramakrishnan, V. (2001) Recognition of cognate transfer RNA by the 30S ribosomal subunit. *Science* 292**:**897-902.
6. Ogle, J. M., Murphy, F. V., Tarry, M. J. & Ramakrishnan, V. (2002) Selection of tRNA by the ribosome requires a transition from an open to a closed form. *Cell* 111**:**721-732.
7. Voorhees, R. M., Weixlbaumer, A., Loakes, D., Kelley, A. C. & Ramakrishnan, V. (2009) Insights into substrate stabilization from snapshots of the peptidyl transferase center of the intact 70S ribosome. *Nat. Struct. Mol. Biol.* 16**:**528-533.
8. Vitagliano, L., Masullo, M., Sica, F., Zagari, A. & Bocchini, V. (2001) The crystal structure of *Sulfolobus solfataricus* elongation factor 1 alpha in complex with GDP reveals novel features in nucleotide binding and exchange. *EMBO J.* 20**:**5305-5311.
9. Lee, H. H., Kim, Y. S., Kim, K. H., Heo, I., Kim, S. K., Kim, O., Kim, H. K., Yoon, J. Y., Kim, H. S., Kim, D. J., Lee, S. J., Yoon, H. J., Kim, S. J., Lee, B. G., Song, H. K., Kim, V. N., Park, C. M. & Suh, S. W. (2007) Structural and functional insights into Dom34, a key component of no-go mRNA decay. *Mol. Cell* 27**:**938-950.
10. Weeks, C. M. & Miller, R. (1999) The design and implementation of SnB version 2.0. *J. Appl. Crystallogr.* 32**:**120-124.
11. de La Fortelle, E. & Bricogne, G. (1997) Maximum likelihood heavy-atom parameter refinement for multiple isomorphous replacement and multiwavelength anomalous diffraction methods. *Methods Enzymol.* 276**:**472-494.

12. Abrahams, J. P. & Leslie, A. G. W. (1996) Methods used in the structure determination of bovine mitochondrial F-1 ATPase. *Acta Crystallogr.* D52**:**30-42.
13. Cowtan, K. D. & Zhang, K. Y. J. (1999) Density modification for macromolecular phase improvement. *Prog. Biophys. Mol. Biol.* 72**:**245-270.
14. Terwilliger, T. C. (2000) Maximum-likelihood density modification. *Acta Crystallogr.* D56**:**965-972.
15. Emsley, P. & Cowtan, K. (2004) Coot: model-building tools for molecular graphics. *Acta Crystallogr.* D60**:**2126-2132.
16. Adams, P. D., Grosse-Kunstleve, R. W., Hung, L. W., Ioerger, T. R., McCoy, A. J., Moriarty, N. W., Read, R. J., Sacchettini, J. C., Sauter, N. K. & Terwilliger, T. C. (2002) PHENIX: building new software for automated crystallographic structure determination. *Acta Crystallogr.* D58**:**1948-1954.
17. Ito-Harashima, S., Kuroha, K., Tatematsu, T. & Inada, T. (2007) Translation of the poly(A) tail plays crucial roles in nonstop mRNA surveillance via translation repression and protein destabilization by proteasome in yeast. *Genes Dev.* 21**:**519-524.
18. Dimitrova, L. N., Kuroha, K., Tatematsu, T. & Inada, T. (2009) Nascent Peptide-dependent Translation Arrest Leads to Not4p-mediated Protein Degradation by the Proteasome. *J. Biol. Chem.* 284**:**10343-10352.
19. Sanner, M. F., Olson, A. J. & Spehner, J. C. (1996) Reduced surface: An efficient way to compute molecular surfaces. *Biopolymers* 38**:**305-320.
20. Pei, J. M., Kim, B. H. & Grishin, N. V. (2008) PROMALS3D: a tool for multiple protein sequence and structure alignments. *Nucleic Acids Res.* 36**:**2295-2300.
21. Nissen, P., Thirup, S., Kjeldgaard, M. & Nyborg, J. (1999) The crystal structure of Cys-tRNA(Cys)-EF-Tu-GDPNP reveals general and specific features in the ternary complex and in tRNA. *Struct. Fold. Des.* 7**:**143-156.